

## Spin-polarized angle-resolved photoemission study of the electronic structure of Fe(100) as a function of temperature

E. Kisker,\* K. Schröder, W. Gudat, and M. Campagna

*Institut für Festkörperforschung der Kernforschungsanlage Jülich, Postfach 1913, D-5170 Jülich, West Germany*

(Received 4 June 1984)

By spin- and angle-resolved photoemission with synchrotron radiation the electronic structure of Fe(100) has been tested between room temperature and the Curie temperature  $T_C$  for photon energies in the range 20–70 eV. The spin-resolved energy-distribution curves (SREDC's) reflect the dispersions of the  $\Delta_3^1$ -symmetry initial-state bands. This manifests in an abrupt change in spin character of the peak near  $E_F$  from predominantly minority spin to majority spin when tuning the photon energy across 33 eV. The non-spin-resolved EDC's thereby remain nearly unchanged. Upon heating to  $0.85 T/T_C$ , depending on photon energy, qualitative different changes in the SREDC's are observed: At  $h\nu=60$  eV,  $\Gamma_{25}^1$  is found to be stationary in energy upon heating, and the spin-summed intensity decreases by less than 5%. At  $\Gamma_{25}^1$ , a strong loss of intensity occurs. In contrast, at  $h\nu=31$  and 21 eV, an increase in minority-spin (and total) photocurrent upon heating is observed. This is interpreted as resulting from a decrease of the exchange splitting with temperature near  $H$ .

### I. INTRODUCTION

The electronic structure, at finite temperatures, of the 3d transition metals Fe, Co, and Ni is currently a matter of strong theoretical interest. One of the problems is to calculate the Curie temperature ( $T_C$ ), which is known to be much smaller than estimated from the magnitude of the ferromagnetic exchange splitting. This is in contrast to the fact that spin-polarized band theory based on the self-consistent local-density-functional description gives an adequate account of the ferromagnetic ground state (e.g., cohesive energy, nonintegral moments).<sup>1</sup> The basic common idea behind present theories is to allow for the existence of local magnetic moments even above  $T_C$ .<sup>2–6</sup> The ferromagnetic-to-paramagnetic phase transition is then governed by thermal disordering of the moments, requiring much less energy than single-particle spin flips which would involve energy changes as large as the exchange splitting. The controversy centers around the spatial extent of correlation among the magnetic moments, which is connected intimately to the present debate on the existence of spin waves about  $T_C$ .<sup>7,8</sup>

It has been pointed out recently that a strong indication for the persistence of *unchanged* local moments to temperatures above  $T_C$  is found in the magnetovolume effect of Fe and Ni,<sup>9</sup> i.e., it is the absence of a strong lattice contraction, which, from band theory is expected to occur with the loss of spontaneous magnetization.<sup>1</sup> This, at first glance, would be regarded as *support* of present theories which involve local magnetic moments. However, magnetovolume-effect data, together with specific-heat data, infer that the magnetic moment does not change at all between  $T=0$  and above  $T_C$ .<sup>9</sup> This, for Ni, is in contradiction to any calculations which predict a decrease of the magnetic moment of at least 25% between  $T=0$  and  $T_C$ . No explanation for this fundamental discrepancy is known.<sup>9</sup>

Since photoemission, and especially angle-resolved

photoemission, from clean single crystals probes the electronic structure in a rather direct way, it has been tried in many works to observe changes in the spectra when heating the sample to  $T_C$  and higher.<sup>10,11</sup> Although the electron spin has not been measured in these experiments, exchange-split states have been identified, and a decrease of the exchange splitting up to  $T/T_C=0.94$  of about 20% has been inferred. However, only by actually measuring the electron spin can exchange-split bands be identified unambiguously and the band dispersions detected for Fe(100), as will be shown below. Furthermore, the spin dynamics at elevated temperatures, as spin rotations around the spontaneous magnetization direction or flips of local magnetic moments which currently are considered to be the driving force for the ferromagnetic to paramagnetic phase transition, can only be observed if the spin state is actually resolved in the photoemission experiment. A preliminary account of the present work<sup>12</sup> shows also that the *primary* photocurrent (as distinguished from the inelastic contribution) might not be conserved upon heating in an angle-resolved experiment due to an initial-state- (and binding-energy-) dependent broadening of the photoemission cone. The new data on Fe, furthermore, show for the first time experimentally that the temperature-induced changes in the energy-distribution curves (EDC's) depend on the initial-state wave vector.

### II. TIME SCALE OF THE EXPERIMENT

The result of an experiment on ferromagnets depends on the probing time.<sup>13</sup> Phenomenologically, the physical processes occurring at finite temperatures might be characterized by two different time scales.<sup>13,5</sup> Electron hopping times are of the order of  $h/W \cong 10^{-15}$  sec, where  $W$  is the bandwidth. On this time scale the formation of magnetic moments occurs. The magnetic configuration then fluctuates on a time scale of the order of spin-wave frequencies, which is typically of order  $h/(0.05 \text{ eV}) \cong 10^{-13}$

sec. Little information is current available on the photoelectron probing time. We may estimate it from the width of the states as observed in the experiment, which varies from 0.6 eV slightly below  $E_F$  to about 2 eV at 3 eV binding energy for Fe.<sup>14</sup> This corresponds to lifetimes of the order of  $10^{-14}$  sec. Hence the photoemission probing time is expected to be *intermediate* between the electron hopping time and the spin-fluctuation time. The experiment will therefore depict a temporary image of the microscopic magnetic configuration, averaged over all configurations which occur during the long measuring time within the spatial extent of the light spot at the sample. We note that a similar average is calculated in recent theories based on the disordered-local-moment (DLM) model for ferromagnetism at finite temperatures.<sup>5</sup>

### III. APPARATUS AND EXPERIMENTAL DETAILS

#### A. Light optics

The experiment is similar to a recent one on Ni(110) (Ref. 15) in which a resonance lamp was employed. However, for being able to follow the band dispersions, we used monochromatized, tunable synchrotron radiation from the new German storage ring BESSY in West Berlin. To accomplish most simple experimental conditions, the apparatus was designed to operate with *s*-polarized (normal incident) light. The beamline consisted of a first mirror which focused the synchrotron radiation onto the entrance slit of the toroidal-grating monochromator. The latter has been described in detail elsewhere.<sup>16</sup> By means of an additional mirror, the monochromatized light emerging from the exit slit was imaged onto the sample, after being bent to the electron-optical axis by means of a plane mirror (see Fig. 1). The light-spot size on the sample was

smaller than  $(0.5 \text{ mm})^2$ , matching closely the electron-spectrometer acceptance. In order to be able to compensate for the uncertainty in the position of the light spot on the sample after changes in the BESSY beam optics, the mirror angle (see Fig. 1) with respect to the electron-optical axis was made adjustable under operating conditions by means of a linear-motion feedthrough.

#### B. Characteristics of the electron spectrometer

The photoelectron spectrometer was based on a  $90^\circ$  spherical condenser of 15 mm mean radius. Total-energy resolution, including the linewidth of the light, was 0.4 eV at  $h\nu=60$  eV, decreasing to about 0.25 eV at  $h\nu=21$  eV. The angular acceptance was confined to normal emission with a geometrical limitation at the source of  $\neq 6^\circ$ . Further restrictions were obtained electron-optically inside the electron spectrometer. These restrictions depend on the electron energy since the trajectories achieve larger distances from the axis when the starting energy is larger.<sup>17</sup> The effective angular acceptance is estimated to be smaller than  $\pm 3^\circ$  at 60 eV and  $\pm 5^\circ$  at 20 eV. Changes in the width of the photoelectron-emission cone could be detected by sweeping the electron beam across the entrance slit of the energy analyzer. Since, for optimal beam transmission, the emitting area is imaged onto this aperture, an increase in the width of the image occurs due to spherical aberrations. We note that, due to the well-defined electron-optical conditions, virtually no stray electrons from apertures inside the spectrometer were detected, although several lens elements were hit by stray light.

The energy-distribution curves were scanned by applying a ramp voltage to the photocathode. This has the advantage that the electron-optical focusing conditions are kept unchanged when electrons with different binding (starting) energies are selected.<sup>17</sup>

#### C. Spin-analysis

The spin polarization was measured by means of a Mott detector after accelerating the angle- and energy-selected electrons to 100 keV. For determining the spin sensitivity, two gold-foil targets, about 3000 and 500 Å thick, were employed. The targets were mounted on a motor-operated linear-motion feedthrough for selectively placing them into the beam path. The electrons were detected by surface-barrier detectors, and the preamplified pulses were decoupled from the high voltage by means of fiber-optic transmitters. The detector acceptance angle was confined to an opening angle of 0.4 (rad). Using the thicker gold foil, the count rate in the polarization-sensitive detectors was  $10^{-3}$  times the count rate of a detector in the direct beam path after removing the gold target. Count rates as high as 250 counts/sec in the polarization-sensitive detectors have been obtained after 250-mA BESSY beam injection with the so-called Metro optics in the *d*-band peak at 60 eV photon energy.

#### D. Electronic control

The photoelectron spectrometer was controlled by a microcomputer (CBM 8032) which steered most of the spec-

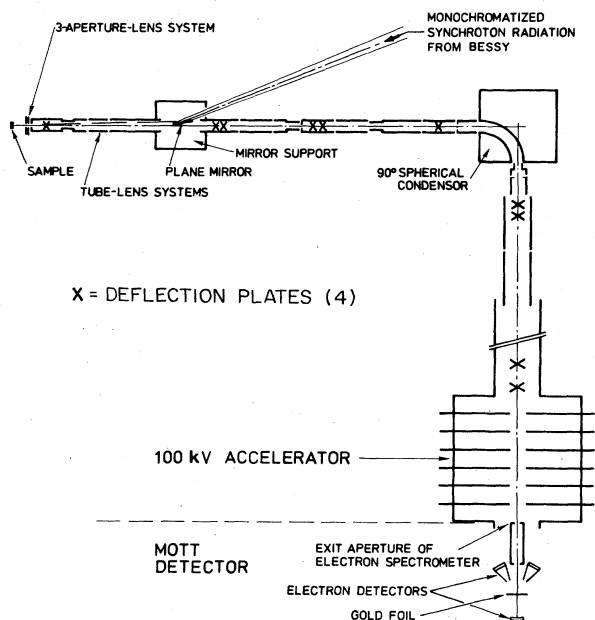


FIG. 1. Schematic of the apparatus for spin-, angle-, and energy-resolved photoemission with synchrotron radiation.

trometer lens and deflection voltages via digital-to-analog converters (total, 28). The EDC's were accumulated in the multiscaling mode. For each voltage step that was output by the microcomputer when measuring the EDC's, four counters were read out and stored by the microcomputer. Three of these counters were connected to electron detectors in the spin analyzer. Two of them (under  $\pm 120^\circ$  scattering angle) served as spin analyzers. The third detector was employed for monitoring the beam transmitted through the gold target foil. The gold foil could be removed from the beam path to obtain the spin-averaged EDC with better statistics than that from the sum of the left and right detectors, and also to obtain a signal with good statistics when computer-optimizing the electron spectrometer.<sup>18</sup> The fourth channel was used to monitor the photon flux during the measurements. This signal was derived from the total photocurrent of the refocusing mirror behind the exit slit of the optical monochromator by means of a voltage-to-frequency converter. During data acquisition the data could be transferred to a second microcomputer (Commodore C64) which provided on-line display of the data. The spin-resolved EDC's (SREDC's) were calculated there and divided by the contents of the photon-flux channels. This served for correcting the data for the steady (and sometimes discontinuous) decrease of the BESSY photon flux, and enabled the detection of relative intensity changes in the SREDC's occurring when the sample was heated.

#### E. The Fe(100) sample

The sample was shaped as a thin disk, 0.4 mm thick and 6 mm in diameter, and had been spark-eroded from a high-purity single crystal of bcc Fe. It was mechanically polished and cleaned *in situ* by standard surface-analysis techniques. Its surface conditions were monitored by low-energy electron-diffraction and photoelectron spectroscopy at photon energies below 30 eV, where the most common surface contaminants, S, C, N, and O, have large cross sections at binding energies between 4 and 6 eV.<sup>19</sup> The sample was mounted with the easy-magnetization direction [001] parallel to the spin-polarization-sensitive axis of the Mott (spin) analyzer, and was magnetized in this direction. The sample could be heated by radiative heating from a bifilar wound tungsten filament from the back side. A tungsten sheet served for heat reflection. The temperature was measured by means of a thermocouple spot-welded to the sample.

Prior to the measurements, the clean sample was annealed for 2 min at 800 K, and after being allowed to cool, was transferred into a small internal magnetizing coil and magnetizing current pulses were applied. Then the room-temperature measurements were performed, preferably after new BESSY beam injection to ensure the shortest possible measuring times. A measuring time of less than 20 min was chosen generally for taking the SREDC's. Then the sample was heated and the elevated-temperature EDC's subsequently taken. Spin-averaged EDC's could be taken in about 2 min with the gold target foil removed from the beam path in the Mott detector. The temperature-induced intensity changes in the

SREDC's, reported below, have been confirmed by comparing them with the more rapidly measured spin-averaged EDC's. Further checks have been made by repeating the measurements after allowing the sample to cool.

#### F. Spin-resolved energy-distribution curves (SREDC's)

From the left and right count rates  $I_1$  and  $I_2$  of the Mott detector, corrected for the apparatus asymmetry as determined from a measurement with a nonmagnetic target ( $I_2 = 0.891I_1$  for unpolarized electrons), the spin-resolved energy-distribution curves  $I^\uparrow(E)$  and  $I^\downarrow(E)$  are obtained as

$$I^{\uparrow,\downarrow} = 0.5 \left[ I \pm \frac{I_1 - I_2}{S_{\text{eff}}} \right]. \quad (1)$$

$S_{\text{eff}}$  is the value of the foil-thickness-corrected Sherman function and  $I$  is the spin-summed count rate. As mentioned above, the SREDC's are normalized to the light intensity at any selected photon energy to detect the transfer of electrons from one spin state into the other one occurring at elevated temperatures.

We note that the spin is measured in the laboratory frame, and  $\uparrow$  refers to electrons with their magnetic moments parallel to the spontaneous-magnetization direction. This labeling, at low temperature, is consistent with the labeling used previously in angle-resolved photoemission. At elevated temperatures, angle-resolved photoemission data implicitly have had their spin labeled according to the temporary direction of a hypothetical local magnetization, which might fluctuate in time and space. Our spin-resolved data at elevated temperatures are also labeled according to the spontaneous-magnetization direction, which remains fixed below  $T_C$ .

#### G. Temperature effects on the spin polarization

Owing to the loss of spontaneous magnetization above  $T_C$ , SREDC's become equal at and above  $T_C$ . The information on the changes in the microscopic electronic structure is contained in the way they approach each other. This might occur principally in two ways: (i) When the exchange splitting is reduced at elevated temperature purely by Stoner-like band shifts, this will result in shifts of the exchange-split peaks in the SREDC's until the peak positions coalesce at  $T = T_C$ . Simultaneously, the spin-summed EDC becomes narrower due to the line shifts. (ii) When constant magnetic moments tend to precess due to thermal disorder under angle  $\theta$  with respect to the spontaneous-magnetization direction, this will result in a balancing of losses in one spin state by gains in the other one. This is because an electron in a pure spin state with respect to a hypothetical *local* magnetization direction will be detected with probability  $\cos^2\theta/2$  in one channel of the spin analyzer and with probability  $\sin^2\theta/2$  in the other. The spin-summed EDC would remain unchanged if the rotation is the only effect since  $\sin^2\theta/2 + \cos^2\theta/2 = 1$ . The rotation includes also the special case  $\theta = 180^\circ$  corresponding to alternating magnetic moments.

From the spin-resolved intensities  $I^\uparrow$  and  $I^\downarrow$ , the spin polarization can be calculated as

$$P = (I^\uparrow - I^\downarrow) / (I^\uparrow + I^\downarrow),$$

and it is also

$$I^{\uparrow,\downarrow} = 0.5(I^\uparrow + I^\downarrow)(1 \pm P).$$

The spin polarization is closely related to the spontaneous magnetization  $M(T)$  and becomes zero at  $T = T_C$  for any binding energy. The quantitative dependence between  $P(T)$  and  $M(T)/M(0)$  is not *a priori* clear since it might depend on the details of the changes of the electronic structure. If no energy shift of the electronic states occurs and the decrease in magnetization is purely due to disordering of constant magnetic moments, the relative spin polarization is  $P(T)/P(0) = M(T)/M(0)$  at any constant binding energy. This follows from the above-mentioned spin-transformation properties.<sup>20</sup> If the local electronic structure also changes, a more general expression is expected,<sup>21</sup>

$$P(T, E) = P_L(T, E) [M(T)/M(0)]. \quad (2)$$

$P_L(E, T)$  is the local spin polarization with respect to the direction of the hypothetical local magnetization. In this case,  $P(T)/P(0)$ , taken at constant binding energy, does not follow the decrease of the relative spontaneous magnetization  $M(T)/M(0)$ . When  $P_L(T, E)$  is independent of temperature,  $I^{\uparrow,\downarrow} = 0.5I_0[1 \pm M(T)/M(0)]$ , and the intensity changes symmetrically around  $I_0$ . Otherwise, the intensity might change asymmetrically.

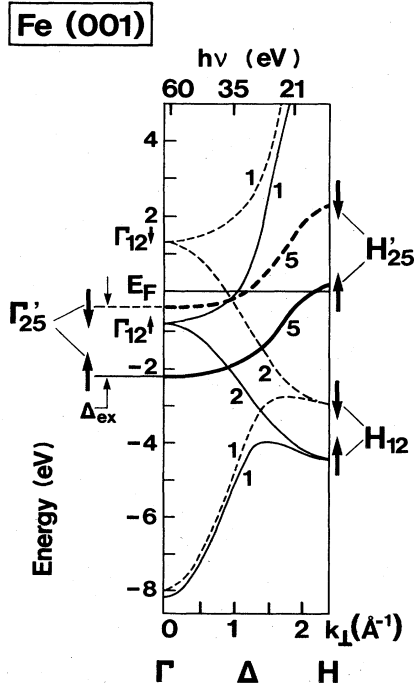


FIG. 2. Band structure of Fe along the  $\Gamma$ - $H$  direction in the Brillouin zone sampled by the present experiments (Ref. 23). The energy scale at the top of the figure indicates the initial-state  $k$  vector ( $k_\perp$ ) for the phototransition from the  $\Delta_5^+$  band.

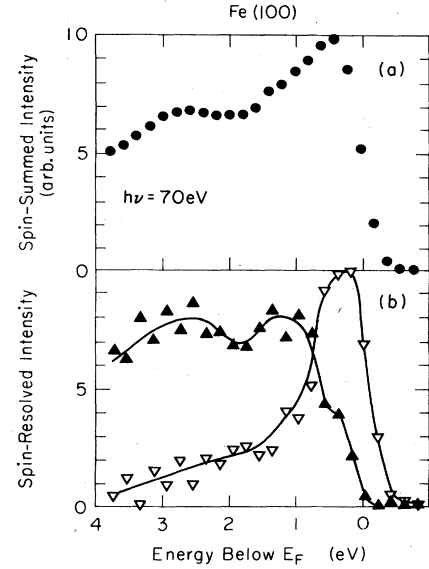


FIG. 3. (a) Spin-summed and (b) spin-resolved energy-distribution curves from Fe(100) for  $s$ -polarized light and normal emission at 70 eV photon energy.  $\blacktriangle$  denotes majority-spin ( $\uparrow$ ) EDC;  $\nabla$  denotes minority-spin ( $\downarrow$ ) EDC.

#### IV. EXPERIMENTAL RESULTS AND DISCUSSION

##### A. Band dispersions

The interpretation of photoemission spectra is easiest for normal emission since, in this case, the component of the photoelectron wave vector  $\vec{k}$  parallel to the surface ( $k_\parallel$ ) is zero, and only the component  $k_\perp$  perpendicular to the surface is a variable.<sup>22</sup> In the present experiment, the photoelectron acceptance cone is centered around the normal direction, and, therefore, the interpretation of the data might first be sought in terms of normal emission.

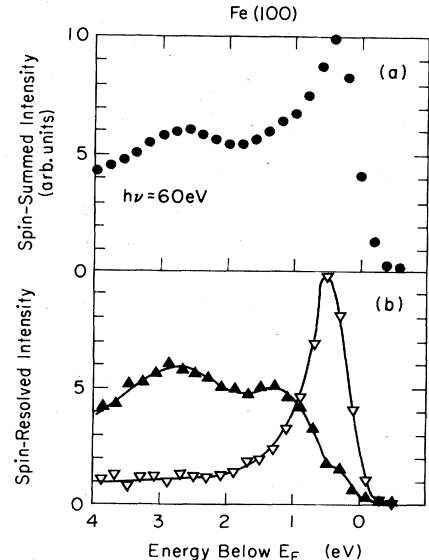
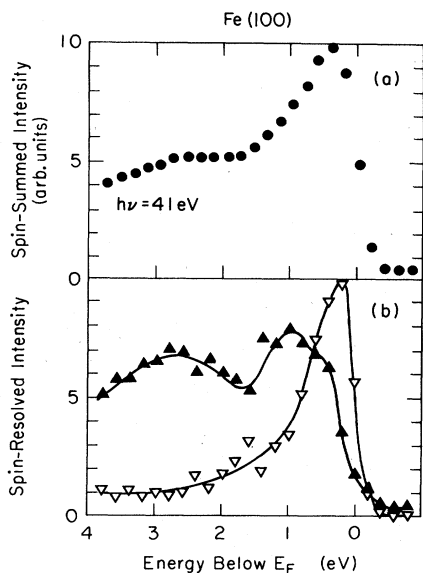
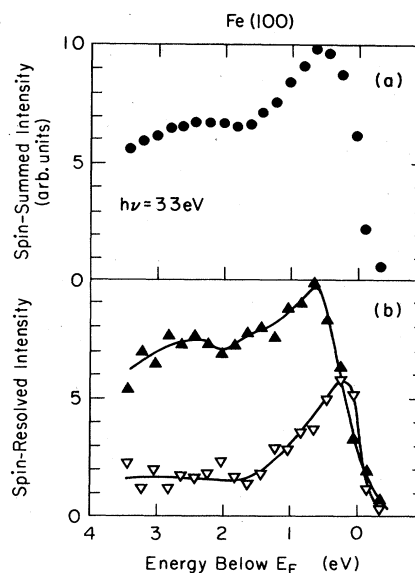


FIG. 4. Same as Fig. 3, except  $h\nu = 60$  eV.

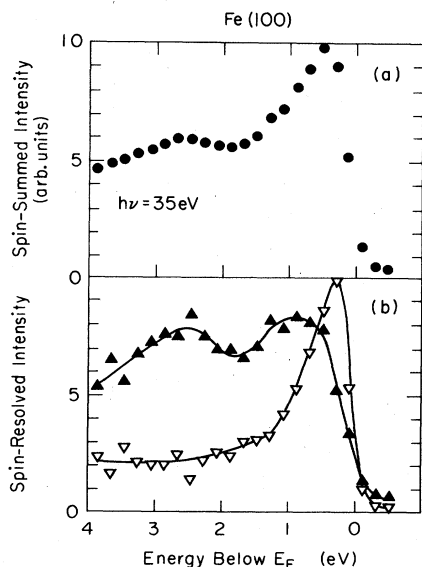
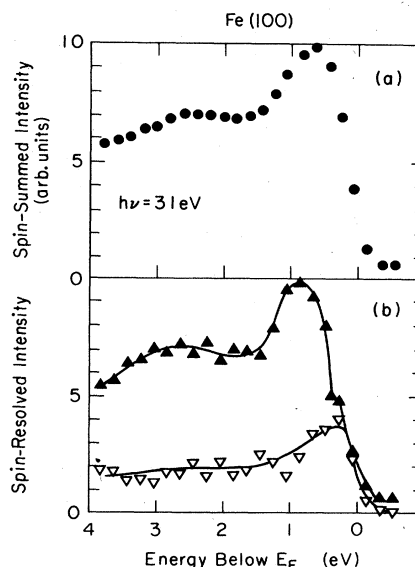
FIG. 5. Same as Fig. 3, except  $h\nu=41$  eV.FIG. 7. Same as Fig. 3, except  $h\nu=33$  eV.

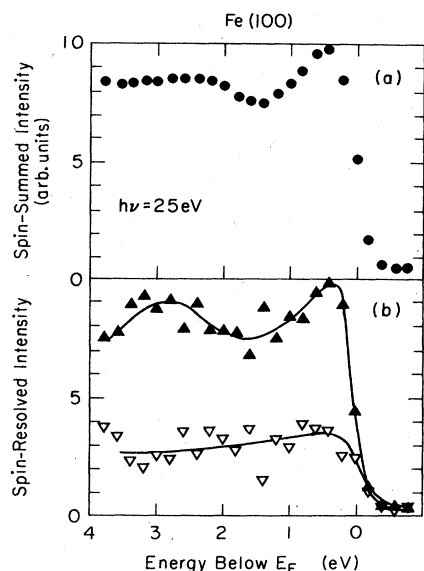
The finite angular acceptance has the effect of additional photocurrent with  $k_{||} \neq 0$ . For structures in the spectra which cannot be explained within normal emission, off-normal contributions therefore might be considered.

Dipole selection rules indicate that only  $\Delta_5$  symmetry bands along the  $\Gamma-H$  direction [see Fig. 2 (Ref. 23)] are allowed as initial states for the Fe(100) surface with  $s$ -polarized light and normal emission. The band dispersions have been studied by measuring spin-resolved and spin-summed EDC's at photon energies between 70 and 20 eV (see Figs. 3–11). The spin-summed EDC's [Figs. 3(a)–11(a)] generally display two peaks, one located near the Fermi energy  $E_F$  and the other at about 2.6 eV binding energy. Except for changes in the relative peak heights and background, there is not much change with

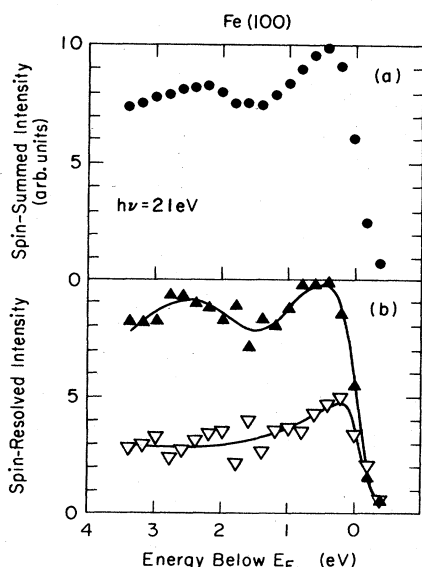
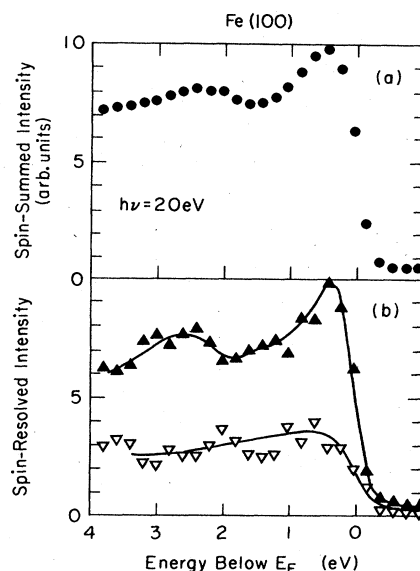
photon energy in the spin-summed EDC's. This observation had been made earlier,<sup>24,25</sup> and from an apparent lack of peak dispersion it was concluded that a (symmetry-projected) density of states is observed.

However, the SREDC's [Figs. 3(b)–11(b)] show that dispersions actually take place. The minority-spin intensity drops strongly between  $h\nu=35$  and 33 eV, indicating that the minority-spin initial state crosses the Fermi energy. Simultaneously, a majority-spin peak grows near  $E_F$ , thereby retaining the peak near  $E_F$  in the spin-averaged EDC. Above  $h\nu=35$  eV the minority-spin initial state is presumably located in the left half of the Brillouin zone.<sup>26</sup> Below 35 eV the minority-spin transition apparently takes place from states where the minority-spin band crosses  $E_F$ , as concluded from the minor influence on photon en-

FIG. 6. Same as Fig. 3, except  $h\nu=35$  eV.FIG. 8. Same as Fig. 3, except  $h\nu=31$  eV.

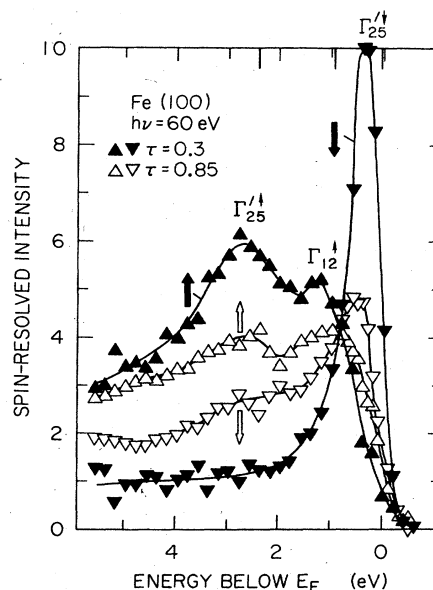
FIG. 9. Same as Fig. 3, except  $h\nu=25$  eV.

ergy between 31 and 20 eV. The  $\downarrow$ -spin phototransition between  $h\nu=31$  and 20 eV probably occurs primarily via indirect transition at  $k$  vectors where the  $\Delta_5^{\downarrow}$  band crosses  $E_F$ . There might also be contributions from states near  $\Gamma$  (corresponding to the  $\uparrow$ -spin peak around  $E_B=2.6$  eV, which is present at any photon energy). The dominating peak in the majority-spin EDC's for photon energies between 31 and 20 eV is interpreted as being due to direct transitions from initial states in the right half of the Brillouin zone. At  $h\nu=31$  eV the  $\uparrow$ -spin transition takes place at about 0.7 of the  $\Gamma-H$  separation, as inferred by comparing the peak position near  $E_F$  in the  $\uparrow$  SREDC with the band structure (Fig. 2). At  $h\nu=21$  eV the transition occurs closer to  $H$ . We note that the direct transi-

FIG. 10. Same as Fig. 3, except  $h\nu=21$  eV.FIG. 11. Same as Fig. 3, except  $h\nu=20$  eV.

tions from the  $\Delta_5^{\downarrow}$  band dominate the SREDC's between  $h\nu=31$  and 20 eV. A not-fully-resolved structure at  $E_F$  appears additionally in many of the  $\uparrow$  SREDC's in Figs. 3(b)–11(b) and is interpreted<sup>26</sup> in terms of a majority-spin surface resonance.

Spin-resolved energy-distribution curves at  $h\nu=60$  eV are shown in Fig. 12 for two different temperatures. The data at  $T/T_C=0.3$  display the features as reported,<sup>27</sup> but are much better resolved. The minority-spin SREDC displays only one single sharp peak (we label it  $\Gamma_{25}^{\downarrow}$ ) ( $0.4\pm 0.2$ ) eV below  $E_F$ . In the majority-spin SREDC two peaks are resolved, one located at a binding energy  $E_B$  of ( $2.6\pm 0.2$ ) eV and the other at ( $1.2\pm 0.2$ ) eV. The peaks at

FIG. 12. Spin-resolved energy-distribution curves at  $h\nu=60$  eV for two temperatures ( $\tau=T/T_C=0.3$  and 0.85).

2.6 and 0.4 eV binding energy are due to emission from the exchange-split  $\Delta_5$ -symmetry bands near the center of the exchange-split  $\Delta_5$ -symmetry bands near the center of the Brillouin zone ( $\Gamma_{25}^{\uparrow}$  and  $\Gamma_{25}^{\downarrow}$ ). The peak at 1.2 eV is due to emission from the  $\Delta_1^{\uparrow}$  band near  $\Gamma$ , which actually is forbidden for strictly normal emission.

### B. Changes in the SREDC's with temperature

Upon heating to  $T/T_C=0.85$ , the following changes are observed (see Fig. 12): In the minority SREDC, the peak  $\Gamma_{25}^{\downarrow}$  diminishes strongly in intensity, while its energy width increases by about a factor of 3, and its peak position shifts by 0.2 eV to larger binding energy. At  $E_B=2.6$  eV, a new broad peak emerges upon heating.

In the majority SREDC, the  $\Gamma_{25}^{\uparrow}$  peak at  $E_B=2.6$  eV loses intensity, but much less than its exchange-split counterpart. Its position remains nearly unchanged. At the peak position of the minority SREDC ( $\Gamma_{25}^{\downarrow}$ ), a small majority-spin intensity gain is observed. We note that the new peak in the  $\downarrow$  SREDC around  $E_B=2.6$  eV seems to be broader than the peak due to  $\Gamma_{25}^{\uparrow}$  in the  $\uparrow$  SREDC.

A marked feature of Fig. 12 is that the binding energy where the up- and down-spin EDC's cross each other is the same for  $T/T_C=0.3$  and 0.85 (and also at intermediate temperatures). In other words, the binding energy  $E_0$  where the spin polarization is zero does not change with temperature, and the total intensity also remains constant at that particular energy. At  $E_0$  no transfer of one spin state into the other occurs upon heating (or, the transfers compensate each other in each spin state). This is a different behavior than around  $E_B=2.6$  eV ( $\Gamma_{25}^{\uparrow}$ ), where only the spin-summed intensity remains (nearly) unchanged. We note also that  $E_0$  is not at the center energy between the exchange-split peaks  $\Gamma_{25}^{\uparrow}$  and  $\Gamma_{25}^{\downarrow}$  due to the presence of emission from  $\Gamma_{12}^{\uparrow}$ .

Spin-summed EDC's (Fig. 13) show more clearly than Fig. 12 that around the  $\Gamma_{25}^{\uparrow}$  peak position only a minor in-

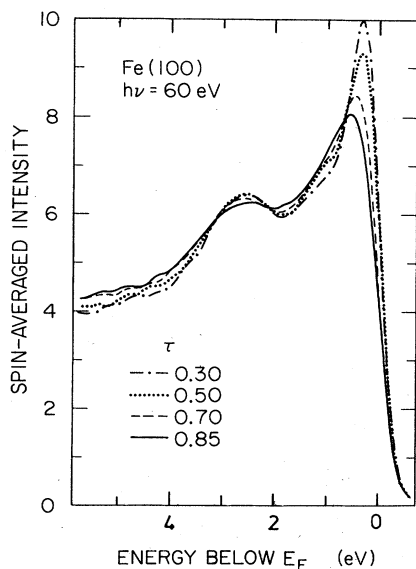


FIG. 13. Spin-summed energy-distribution curves from Fe(100) at  $h\nu=60$  eV taken at different temperatures.

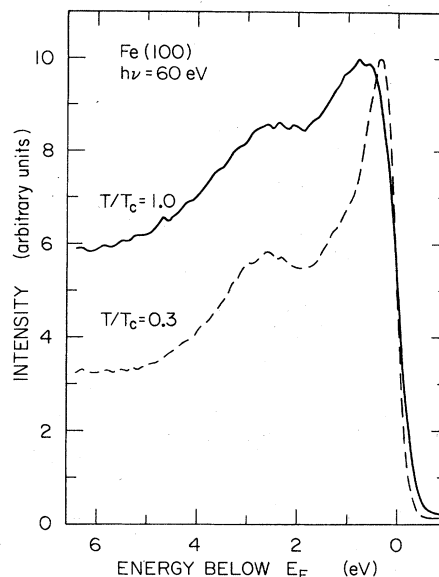


FIG. 14. Spin-summed energy-distribution curves taken at  $T=0.3$  and  $T=T_C$  normalized to equal peak heights for  $h\nu=60$  eV.

tensity decrease occurs between  $T/T_C=0.3$  and 0.85, indicating that losses in the majority SREDC are nearly completely compensated for by the new growing peak in the minority SREDC. (Part of the compensation might also be due to an increased  $\downarrow$ -spin background.) This is not the case at the position of the  $\Gamma_{25}^{\downarrow}$  peak, where the total intensity drops down upon heating because of the stronger losses of minority spins as compared to the gains of majority spins. The decrease in intensity at  $\Gamma_{25}^{\downarrow}$  is also larger than expected from the Fermi-Dirac function.

An EDC taken at  $T=T_C$  is compared with one taken at room temperature in Fig. 14. During heating to this high temperature, S segregation to the surface occurs quickly and the surface certainly is no longer clean. However, upon cooling, the peak positions are the same as in the original EDC at  $T/T_C=0.3$ , and we also observe again an intensity gain near  $E_F$ . Primarily to find the peak position of  $\Gamma_{25}^{\downarrow}$  which is superimposed on a large background, we fitted the EDC at  $T=T_C$  with Lorentzian curves. A good fit is obtained with two Lorentzians and a background contribution as the integral over the Lorentzians (normalized appropriately). The fit gives the peak position of  $\Gamma_{25}^{\downarrow}$  as  $2.6_{-0.5}^{+0.1}$  eV at  $T=T_C$ . Fits of this kind are never unique, but a conclusion would be that  $\Gamma_{25}^{\downarrow}$  remains stationary up to  $T_C$ . The fit around the  $\Gamma_{12}^{\uparrow}$  position with only one Lorentzian is more questionable. It is expected that an even better fit could be obtained with two closely separated Lorentzians. From the decrease in amplitude of  $\Gamma_{25}^{\downarrow}$  up to  $T/T_C=0.85$ , it might be concluded that  $\Gamma_{25}^{\downarrow}$  will become very broad and small in amplitude at higher temperatures. Therefore, the broad peak at  $E_B=0.8$  eV probably is mostly due to an unshifted  $\Gamma_{12}^{\uparrow}$  peak and also due to a remainder of  $I_{25}^{\downarrow}$ .

The balancing of gains and losses in intensity observed at the position of  $\Gamma_{25}^{\downarrow}$  could be interpreted in terms of

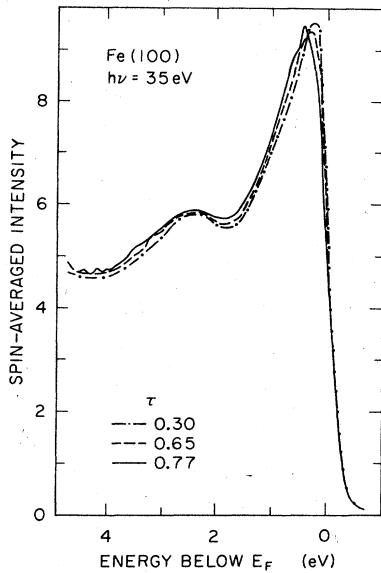


FIG. 15. Spin-summed energy-distribution curves at  $h\nu=35$  eV taken at  $T/T_c=0.3, 0.65,$  and  $0.77$ .

fluctuations of a constant magnetic moment around the spontaneous-magnetization axis, resulting in a mixing of spins in the spin analyzer (even of internally pure spin states with respect to the instantaneous direction of the local moment). However, the different behavior at the position of  $\Gamma_{25}^{\downarrow}$  indicates already that this model is not completely adequate.

For 35 eV, spin-summed EDC's taken at different temperatures are shown in Fig. 15. Compared to the 60-eV data, the intensity changes are small.

In Fig. 16, SREDC's taken at different temperatures for  $h\nu=31$  eV are shown, and in Fig. 17 for  $h\nu=21$  eV.

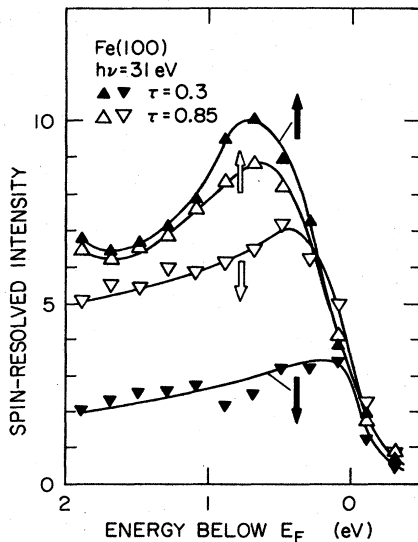


FIG. 16. Spin- and angle-resolved energy-distribution curves of Fe(001) at 31 eV photon energy for  $T/T_c=0.3$  and  $0.85$  (unsmoothed data).

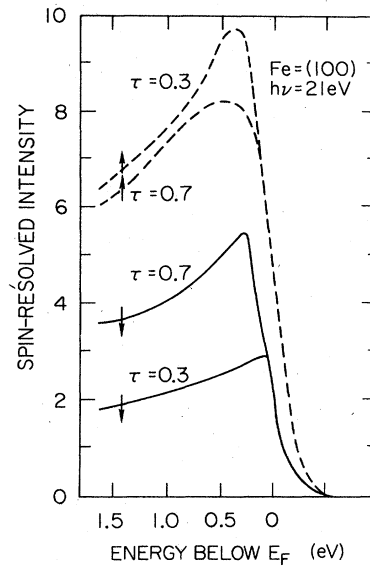


FIG. 17. Spin- and angle-resolved energy-distribution curves of Fe(001) at 21 eV photon energy for  $T/T_c=0.3$  and  $0.7$ .

There is a marked difference to the  $h\nu=60$  eV data (Figs. 12 and 13): Instead of a decrease in spin-summed intensity near  $E_F$ , we observe a strong increase in total photocurrent upon heating for photon energies of 31 and 21 eV. The SREDC's demonstrate that it is a doubling of minority-spin intensity and a comparatively small decrease in majority-spin intensity which causes the gain in total intensity. This asymmetry excludes an interpretation of the majority- and minority-spin intensity changes as transverse fluctuations of a local magnetic moment. We conclude that the reason for the minority-spin intensity increase upon heating is a buildup of the minority-spin density of states at and slightly below  $E_F$  near  $k$  vectors where the  $\uparrow$ -spin phototransition occurs efficiently ( $\sim 0.7$  of the  $\Gamma$ - $H$  separation at 31 eV). This would allow for direct transitions for  $\downarrow$  electrons from these temperature-

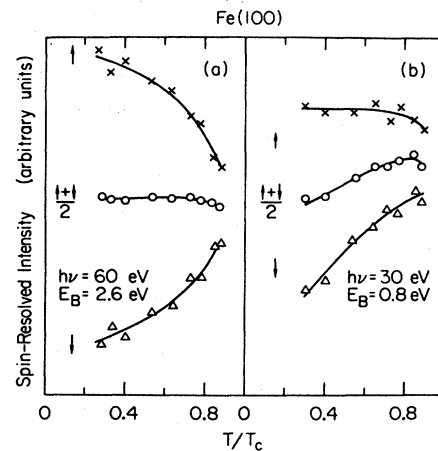


FIG. 18. Spin-resolved intensities as function of temperature for (a)  $h\nu=60$  eV and  $2.6$  eV binding energy ( $\Gamma_{25}^{\downarrow}$ ) and for (b)  $h\nu=30$  eV and  $E_B=0.8$  eV.



induced initial states with the result of an increase in  $\downarrow$  photocurrent. The majority-spin phototransition does not suffer from the Fermi energy cutoff, explaining its less pronounced temperature dependence. However, its intensity decreases, which could be explained by an upwards shift of the majority-spin band.

The different character of the spin rearrangement upon heating is seen again in Fig. 18, where the spin-resolved intensities taken at a constant binding energy are shown for two cases,  $h\nu=60$  eV,  $E_B=2.6$  eV, and  $h\nu=30$  eV,  $E_B=0.8$  eV. The balancing of spins for the first case is in agreement with the above-mentioned findings on the behavior of  $\Gamma_{25}^{\uparrow}$ , and the increase in  $\downarrow$  intensity is in accordance with the data in Fig. 16.

### C. Changes in angular width with temperature

A reason for the strong intensity loss upon heating at the position of  $\Gamma_{25}^{\downarrow}$  is the increase in angular width of the photoemission cone, which is sharply peaked to the normal direction at low temperature. This is seen in Fig. 19, where the beam profiles obtained by sweeping the beam across the entrance aperture of the electron-energy analyzer are compared for two different temperatures. The electron spectrometer was set to fixed binding energy (equal to the Fermi energy in this case). The larger width  $\Delta U$  in deflection voltage reflects a broader image of the emitting area on the aperture over which the beam is swept. The increase in width  $\Delta U$  is due to geometrical aberrations of the electron lens systems, and  $\Delta U=C\Delta\alpha^3$ .<sup>28</sup> The constant  $C$  is presently being calculated from the computed trajectories.

Only a very small increase in angular width with temperature is observed at the position of the majority-spin peak ( $\Gamma_{25}^{\downarrow}$ ) upon heating, in agreement with the stated nearly-constant spin-summed intensity.

Since the photoelectron-emission angle is determined by

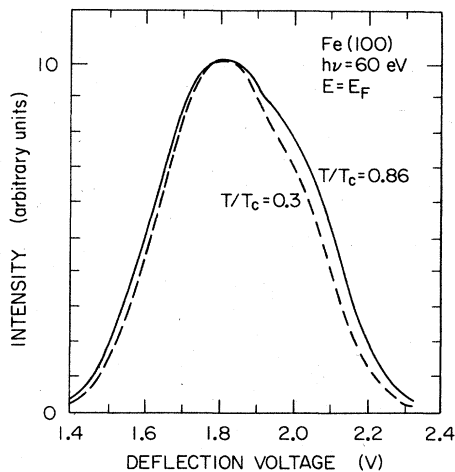


FIG. 19. Beam profile obtained when sweeping the electron beam across the entrance aperture of the electron spectrometer by ramping the voltage across a set of deflection plates in front of the aperture, at two different sample temperatures ( $T/T_C=0.3$  and  $0.85$ ).

the internal  $k$  vector, the broadening is interpreted as a  $\vec{k}$  broadening of the initial state. The  $\vec{k}$  broadening is connected to the energy broadening by the relation  $\Delta k = \Delta E(\partial k / \partial E)$ .<sup>29</sup> Since  $\Gamma_{25}^{\downarrow}$  is broadened in energy much more than  $\Gamma_{25}^{\uparrow}$ , the  $\vec{k}$  broadening of  $\Gamma_{25}^{\downarrow}$ , much stronger than  $\Gamma_{25}^{\uparrow}$ , can also be understood.

### D. Surface magnetism

We have plotted in Fig. 20 the relative spin polarization  $P(T)$  corresponding to the data in Fig. 18 as function of temperature, normalized to an extrapolated  $P(0)=1$ . Also indicated in the figure are calculations of the layer-dependent magnetization as function of temperature. The calculations were performed in the mean-field approximation with equal interlayer and intralayer coupling constants in a manner similar to that of Wolfram *et al.*<sup>30</sup> It is seen that  $P(T)$  behaves much like the first- to second-layer magnetization temperature dependence. For  $h\nu=30$  eV [Fig. 20(b)], it is actually closely to the first-layer magnetization. This behavior, however, might be accidental, and could be an indication of the validity of Eq. (2), since the changes in polarization are due to the strong minority-current increase, which has been interpreted above as an effect due to the buildup of  $\downarrow$ -spin states around  $k=0.7$  along  $\Gamma-H$ .

### E. Comparison with the disordered-local-moment theory

We have seen in the preceding subsection that the data most probably represent the magnetic properties of just a few (1–3) surface crystal planes. However, the room-temperature data can be interpreted based primarily on the bulk electronic structure, indicating that intrinsic sur-

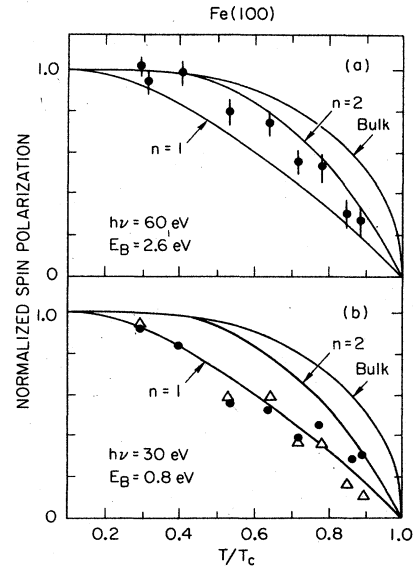


FIG. 20. Spin polarization as function of temperature taken (a) at 2.6 eV binding energy ( $\Gamma_{25}^{\downarrow}$ ) at  $h\nu=60$  eV, and (b) at 0.8 eV binding energy at  $h\nu=30$  eV. The data are normalized to the room-temperature spin polarization.

face effects are small. We might therefore expect that the finite-temperature properties can also be interpreted at least qualitatively from predictions for the bulk.

The only present self-consistent theory which makes quantitative predictions on the changes in electronic structure with temperature, is the disordered-local-moment theory.<sup>5,31</sup> Within this theory, the electronic structure of Fe above  $T_C$  has been calculated from first principles in the Korringa-Kohn-Rostoker coherent-potential approximation (KKR-CPA), treating ferromagnetism at finite temperature as a binary-alloy problem, and the correct Curie temperature has been obtained, for example.<sup>5,29</sup> Within this theory, the so-called Bloch spectral function  $A_B(k, E)$  has also been calculated,<sup>5,31</sup> a quantity which can be interpreted as the density of states per  $k$  point, i.e., at  $T=0$ ,  $A_B(k, E)$  is a  $\delta$  function at the Bloch-energy eigenvalues. At finite temperatures,  $A_B(k, E)$  generally becomes smeared out in  $k$  and  $E$  as a result of disorder. One of the predictions that was made was that  $\Gamma_{25}^{\downarrow}$  is nearly stationary in energy (a shift of about 0.7 eV has been predicted,<sup>5,29</sup> as compared to the exchange splitting at  $\Gamma$  of 2.2 eV), whereas at  $H$  the exchange splitting should vanish above  $T_C$ . The decrease in the exchange splitting leads to a large amplitude of the Bloch spectral function at  $E_F$  around 0.7 of the  $\Gamma$ - $H$  separation above  $T_C$ .<sup>31</sup> At  $T=0$ , it would have a large amplitude only where the  $\Delta_5^{\downarrow}$  bands cross  $E_F$ , i.e., at 0.9 and 0.5 of the  $\Gamma$ - $H$  separation, respectively (see Fig. 2). This buildup of density of states would appear gradually (proportional to the decrease of the spontaneous magnetization) with temperature. Furthermore, a strong broadening at  $\Gamma_{25}^{\downarrow}$  in both  $k$  and energy with temperature has been predicted.<sup>29</sup> This would lead to a strong decrease in intensity at this binding energy in an angle- and energy-resolved photoemission experiment.

Upon comparison with the experimental data discussed above, we conclude that some of these predictions are qualitatively fulfilled. This is most obvious for the data taken near  $\Gamma$  ( $h\nu=60$  eV), although the shift of  $\Gamma_{25}^{\downarrow}$  experimentally seems to be smaller than predicted.<sup>32</sup> We also observed the strong broadening at  $\Gamma_{25}^{\downarrow}$  in energy and angle ( $\vec{k}$ ). The predicted buildup of the Bloch spectral function around 0.7  $\Gamma$ - $H$  at and below  $E_F$  is seen most elucidly in the increase of minority-spin photocurrent in

the data taken at  $h\nu=31$  and 21 eV, Figs. 16 and 17. The phototransition would "like" to occur as effectively for minority-spin electrons as for majority ones, but at room temperature, the minority band in the right half of the Brillouin zone, where the majority-spin phototransition takes place, is located above  $E_F$ . The strong increase in minority-spin photocurrent upon heating is therefore interpreted as a buildup of the minority-spin initial density of states upon heating, in agreement with the calculations in the disordered-local-moment picture.

## V. CONCLUSION

The new data might serve as a test for quantitative calculations. A finite-temperature theory of ferromagnetism (and of the photoemission process) must simultaneously explain the nearly stationary character of  $\Gamma_{25}^{\downarrow}$ , the  $\vec{k}$  broadening at  $\Gamma_{25}^{\downarrow}$ , and, the apparent shift of the  $\Delta_5^{\downarrow}$  band for large  $k$  vectors. The data also demonstrate that the photoelectron energy distribution might become deformed at high temperatures due to binding-energy-dependent losses of photoemission intensity as a consequence of fixed angular acceptance.

*Note added.* Recently, it has been shown [V. Korenman and R. E. Prange, Phys. Rev. Letters 53, 186 (1984)] that the temperature dependence of the observed exchange splitting depends on the effective mass of the hole and, hence, on the  $k$  vector. For a brief discussion of phonon effects at elevated temperatures see: E. Kisker, J. Magn. Magn. Mater. 45, 23 (1984).

## ACKNOWLEDGMENTS

We would like to acknowledge fruitful and stimulating discussions with J. Callaway, D. M. Edwards, B. L. Gyorffy, R. Feder, M. B. Stearns, and G. M. Stocks, and we thank Ing D. Hoffmann for his excellent technical support. We gratefully acknowledge the technical support of the BESSY staff. One of us (E.K.) wishes to thank E. L. Garwin for the hospitality at the Stanford Linear Accelerator Center (SLAC) during preparation of this paper. This work was supported by the U.S. Department of Energy under Contract NO. DE-AC03-76SF00515.

\*On sabbatical leave to Stanford Linear Accelerator Center, Stanford University, Stanford, CA 94305.

<sup>1</sup>D. E. Eastman, J. F. Janak, A. R. Williams, R. V. Coleman, and G. Wendin, J. Appl. Phys. 50, 7423 (1979).

<sup>2</sup>H. Capellmann, J. Phys. F 4, 1466 (1974).

<sup>3</sup>V. Korenmann, J. L. Murray, and R. E. Prange, Phys. Rev. B 16, 4032 (1977).

<sup>4</sup>M. V. You, V. Heine, A. J. Holden, P. J. Lin-Chung, Phys. Rev. Lett. 44, 1282 (1980).

<sup>5</sup>B. L. Gyorffy, J. Kollar, A. J. Pindor, J. Staunton, G. M. Stocks, and H. Winter, in Proceedings of the Workshop on 3D Metallic Magnetism, edited by D. Givord and K. R. A. Ziebeck, Institut-Lauve-Langevin (Genoble) Internal Report No. 832I18T, 1983 (unpublished).

<sup>6</sup>H. Hasegawa, J. Phys. Soc. Jpn. 49, 963 (1980).

<sup>7</sup>J. W. Lynn, Phys. Rev. B 11, 2624 (1975).

<sup>8</sup>O. Steinsvoll, C. F. Majkrzak, G. Shirane, and J. Wicksted, Phys. Rev. Lett. 51, 300 (1983).

<sup>9</sup>A. J. Holden, V. Heine, and J. H. Samson, J. Phys. F 14, 1005 (1984).

<sup>10</sup>D. E. Eastman, F. J. Himpsel, and J. A. Knapp, Phys. Rev. Lett. 44, 95 (1978).

<sup>11</sup>A. M. Turner and J. L. Erskine, Phys. Rev. B 25, 1983 (1982).

<sup>12</sup>E. Kisker, K. Schröder, M. Campagna, and W. Gudat, Phys. Rev. Lett. 52, 2285 (1984).

<sup>13</sup>H. Capellmann, J. Magn. Magn. Mater. 28, 250 (1982).

<sup>14</sup>A detailed analysis of the width of structures in photoemission EDC's is in preparation.

<sup>15</sup>H. Hopster, R. Raue, G. Güntherodt, E. Kisker, R. Clauberg, and M. Campagna, Phys. Rev. Lett. 51, 829 (1983).

<sup>16</sup>W. Gudat, E. Kisker, G. M. Rothberg, and C. Depautex, Nucl. Instrum. Methods 195, 233 (1982).

- <sup>17</sup>E. Kisker, R. Clauberg, and W. Gudat, *Rev. Sci. Instrum.* **53**, 1137 (1982).
- <sup>18</sup>K. Schröder (unpublished).
- <sup>19</sup>G. Broden, G. Gafner, and H. P. Bonzel, *Appl. Phys.* **13**, 333 (1977).
- <sup>20</sup>See, for example, D. M. Edwards, *J. Phys. C* **16**, L327 (1983), where a similar expression is derived for spin polarized field emission.
- <sup>21</sup>E. Kisker, *J. Chem. Phys.* **87**, 3597 (1983).
- <sup>22</sup>See, for example, N. V. Smith, in *Photoemission in Solids I*, Vol. 28 of *Topics in Applied Physics*, edited by M. Cardona and L. Ley (Springer, New York, 1978).
- <sup>23</sup>C. S. Wang and J. Callaway, *Phys. Rev. B* **16**, 2095 (1977).
- <sup>24</sup>A. Schultz, R. Courths, H. Schultz, and S. Hüfner, *J. Phys. F* **9**, L41 (1979).
- <sup>25</sup>P. Heimann and N. Neddermeyer, *Phys. Rev. B* **18**, 3537 (1978).
- <sup>26</sup>For a theoretical interpretation in terms of the band structure, see R. Feder, U. Baier, A. Rodriguez, and E. Kisker, *Solid State Commun.* **52**, 57 (1984).
- <sup>27</sup>R. Feder, W. Gudat, E. Kisker, K. Schröder, and A. Rodriguez, *Solid State Commun.* **46**, 619 (1983).
- <sup>28</sup>See, for example, O. Klemperer, in *Electron Optics* (Cambridge University Press, Cambridge, 1953).
- <sup>29</sup>G. M. Stocks (private communication).
- <sup>30</sup>T. Wolfram, R. E. DeWames, W. F. Hall, and P. W. Palmberg, *Surf. Sci.* **28**, 45 (1971).
- <sup>31</sup>J. Staunton, B. L. Gyorffy, A. J. Pindor, G. M. Stocks, and H. Winter (unpublished).
- <sup>32</sup>According to Ref. 31 and recent photoemission calculations in the disordered-local-moment picture [P. J. Durham, J. Staunton, and B. L. Gyorffy, *J. Magn. Magn. Mater.* **45**, 38 (1984)],  $\Gamma'_{25}^1$  and  $\Gamma'_{25}^1$  should coalesce above  $T_C$  at a binding energy about 0.7 eV higher than the energy of  $\Gamma'_{25}^1$  at  $T=0$ . This seems to be difficult to reconcile with the data of Fig. 12.